PHYSICAL REVIEW B VOLUME 26, NUMBER 10 15 NOVEMBER 1982

Optical response of uniaxial semiconductors. III. Optical and electron-energy-loss spectra of Te

H. M. Isomäki and J. von Boehm
Electron Physics Laboratory and Department of General Sciences, Helsinki University of Technology, SF-02150 Espoo 15, Finland

T. Stubb
Electron Physics Laboratory, Helsinki University of Technology, SF-02150 Espoo 15, Finland and Semiconductor Laboratory, Technical Research Centre of Finland, SF-02150 Espoo 15, Finland

(Received 1 March 1982)

The permittivity, reflectivity, absorption coefficient, and electron-energy-loss function of trigonal Te are calculated from 0 to 22 eV with the use of the self-consistent Hartree-Fock-Slater band-structure results and the matrix elements rigorously evaluated in the bulk of the first Brillouin zone. Close agreement is found with experiments. The salient features in the optical and electron-energy-loss spectra are interpreted in terms of the transitions between the band groups. The effect of the local fields on the spectra is estimated to be small. The corrections needed to the spectra of Te to improve the agreement with experiments should be opposite to the local-field and continuum-exciton corrections recently calculated for C, Si, and TlCl. The possible reasons for the differences in the ultraviolet region between the calculated one-electron spectra and the experimental ones of Te, Se, $ZrSe_2$, Si, Ge, GaP, GaAs, InAs, InSb, ZnS, and ZnSe are discussed.

I. INTRODUCTION

The anisotropic small-gap semiconductor, trigonal Te, has in the past been subject to an extensive theoretical and experimental study (see Refs. 1 and 2). However, only two calculations of the polarization-dependent Ehrenreich-Cohen permittivity $\vec{\vec{\epsilon}}=\vec{\vec{\epsilon}}_1+i\,\vec{\vec{\epsilon}}_2$ (Refs. 3–5) of Te have appeared.[6,7] Both of these are of the pseudopotential (PSP) type. Maschke calculated in his empirical PSP (EPSP) study $\vec{\vec{\epsilon}}_2$ up to ~ 10 eV.[6] Starkloff and Joannopoulos calculated in their self-consistent (SC) PSP study $\vec{\vec{\epsilon}}$, the reflectivity, the absorption coefficient, and the electron-energy-loss function up to ~ 13 eV.[7]

A further theoretical examination of the optical and electron-energy-loss spectra of Te and the extension of the calculation to higher energies appear appropriate for several reasons. The response spectra calculated with the true SC wave functions may differ from those calculated with the PSP wave functions.[8] The spectra in the present study are calculated with the true SC [orthogonalized plane-wave (OPW)] eigenstates.[9] The measurement of the reflectivity of Te with the synchrotron radiation shows that the reflectivity exhibits distinct structure several eV above the upper energy limit (~ 13 eV) of the previous theoretical studies.[10] Also, the transitions from the three lowest s-type valence bands have the main effect at these high energies. The role of these s-type states in all the response spectra has not been clarified yet (cf. Ref. 11). Similarly, the plasma peak in the measured electron-energy-loss function of Te appears distinctly above the energy region analyzed theoretically thus far.[10] Detailed calculations of the optical properties of trigonal Se have appeared recently,[12] and it is now, for the first time, also possible to present an extensive comparison between the theoretically analyzed response spectra of Te and Se. By comparing the difference between the calculated and the experimental spectra of Te with the calculated local-field corrections for Te (Ref. 13) and qualitatively with the calculated local-field and continuum-exciton corrections for C,[14] Si,[15] and TlCl,[16] we indirectly gain insight into the effects beyond the one-electron theory without actually calculating them. With reference to the present calculations of Te we also discuss the possible reasons for disagreements found recently in the ultraviolet region between the calculated one-electron and the experimental spectra of Se,[12] $ZrSe_2$,[17] Si,[18–20] Ge, GaP, GaAs,[19,20] InAs, InSb,[19] ZnS, and ZnSe.[20] The fundamental equations and

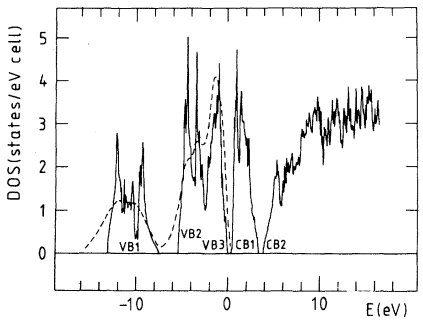

FIG. 1. SCOPW density of states (DOS) of Te (solid line) from Ref. 22. Dashed line represents x-ray photoemission spectrum from Ref. 24. VB1, VB2, VB3, CB1, and CB2 denote *s* bonding, *p* bonding, *p* lone-pair, *p* antibonding, and upper conduction- (lower bands of *d-s* type) band groups, respectively.

the details of the calculation for the present study for Te were given in the first paper[21] of this series, denoted by I hereafter.

II. RESULTS AND DISCUSSION

The primitive unit cell of trigonal Te contains three atoms. The outer atomic *s* and *p* states engender three separate valence-band (VB) triplets and one conduction-band (CB) triplet, which are seen in the calculated density of states (DOS)

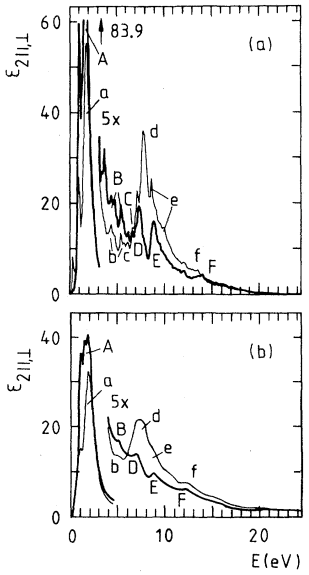

FIG. 2. Imaginary part of the permittivity ($\vec{\epsilon}_2$) of Te. (a) SCOPW $\epsilon_{2\|}$ (thick line) and $\epsilon_{2\perp}$ (thin line). (b) Experimental $\epsilon_{2\|}$ (thick line) and $\epsilon_{2\perp}$ (thin line) from Ref. 10.

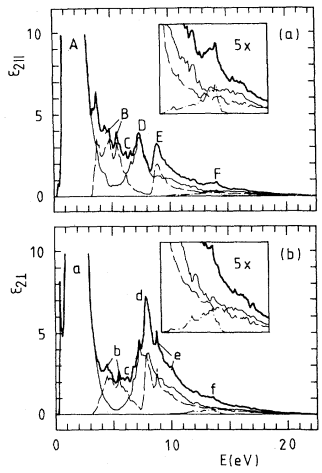

FIG. 3. Triplet decomposition of the SCOPW $\epsilon_{2\|}$ and $\epsilon_{2\perp}$ of Te [(a) and (b), respectively]. Solid thick line corresponds to total $\vec{\epsilon}_2$. Solid, dashed, and dashed-dotted thin lines represent contributions to $\vec{\epsilon}_2$ of transitions from the *p* lone-pair VB3, *p* bonding VB2, and *s* bonding VB1, respectively.

shown in Fig. 1.[22] The valence-band triplets are of *s* bonding (VB1), *p* bonding (VB2), and *p* lone-pair (VB3) type, and the conduction-band triplet is of *p* antibonding (CB1) type (Fig. 1).[9,23] In the higher conduction-band group CB2, the lowest bands are mainly of *d-s* type. The optical and electron-energy-loss spectra of Te will be interpreted in terms of the transitions between the above-mentioned band groups. We compare in Fig. 1 the calculated DOS with the x-ray photoemission spectrum by Schlüter *et al.*[24] and find close agreement.

We present the calculated $\vec{\epsilon}_2$ [consisting of $\epsilon_{2\|}$ and $\epsilon_{2\perp}$, Eq. (47) of paper I, hereafter abbreviated as (I.47)] and the experimental $\vec{\epsilon}_2$ derived by Bammes *et al.*[10] from the reflectivity measured with the synchrotron radiation at 300 K in Figs. 2(a) and 2(b), respectively. Agreement between the calculated and the experimental[10,25,26] $\vec{\epsilon}_2$ is remarkably good (see Fig. 2). The use of the extrapolated reflectivity below 3 eV in Ref. 10 has erroneously caused the disappearing of the optical gap from the experimental $\vec{\epsilon}_2$ in Fig. 2(b). The theoretical $\vec{\epsilon}_2$ is higher than the experimental $\vec{\epsilon}_2$ up to ~ 11 eV and lower above ~ 11 eV. The narrow, calculated first peaks *A* and *a* are significantly higher than the corresponding experimental peaks[25,26] [agreement is better with the peaks measured at the lower temperature of 10 K than with those measured at 300 K (Ref. 26)]. However, this difference does not seem to cause any appreciable disagreement between the heights of the first peaks

TABLE I. Position and origin of the main peaks in $\vec{\epsilon}_2$, the reflectivity, and the absorption coefficient of Te. Transitions causing an appreciable background are in parentheses. All numbers given in eV.

		$\vec{\epsilon}_2$			Reflectivity			Absorption coefficient			
	Peak	Theor.[a]	Expt.[b]	Theor.[c]	Theor.[a]	Expt.[b]	Theor.[c]	Theor.[a]	Expt.[d]	Theor.[c]	Origin[a]
||	*A*	1.5	2.0	1.6	2.9	2.4	2.9	2.4	2.9	2.4	VB3→CB1
	B	4.9	5.0	4.8	5.4	5.4	5.1	5.2	5.7	5.1	VB2→CB1 (VB3→CB1)
	C	6.6		6.6	6.7		6.7	6.6		6.6	VB2→CB1, VB3→CB2
	D	7.3	6.9	7.1	7.8	7.4	7.2	7.7	7.6	7.1	VB3→CB2
	E	8.9	8.7	8.4	10.9	9.5	9.7	9.1	9.6	8.5	VB2→CB2 (VB3→CB2)
	F	14.0	12.0		14.6	12.9		14.1			VB1→CB1 (VB3 + VB2→CB2)
⊥	*a*	1.7	2.1	1.6	3.0	2.4	2.9	2.8	3.0	2.4	VB3→CB1
	b	4.9	4.8	4.8	4.9	5.0	4.8	4.9	5.0	4.8	VB2→CB1 (VB3→CB1)
	c	6.1		6.0	6.1		6.0	6.1		6.0	VB2→CB1, VB3→CB2
	d	7.8	7.3	7.3	8.2	8.0	7.5	8.1	8.2	7.5	VB3 + VB2→CB2
	e	9.3	8.9	9.3	10.1	9.2	10.2	9.4	9.8	9.8	VB3 + VB2→CB2
	f	13.6	12.0		14.2	13.2		13.6			VB1→CB1 (VB3 + VB2→CB2)

[a]Present study.
[b]Peaks *A* and *a* from Ref. 26, others from Ref. 10.
[c]Reference 7.
[d]Reference 26.

in the calculated and measured reflectivities (see below).

The calculated peak positions are compared with the experimental positions[10,26] in Table I. Agreement is close. The cusp at 3.7 eV in the calculated $\epsilon_{2||}$ [Fig. 2(a)] may correspond to the structure embodied in the experimental peak *A* at ~4 eV [Fig. 2(b)]. The tiny shoulders in the experimental $\vec{\epsilon}_2$ at ~16 eV are not discernible in the calculated $\vec{\epsilon}_2$ (Fig. 2). They may be vague images of the shoulders of the measured reflectivity and due to inaccuracies in the Kramers-Kronig transformation (see below). The calculated positions of peaks *F* and *f* differ from the experimental positions (Table I), which may be due to the different convergence rates of distant bands and/or to the sensitivity of the measured reflectivity to surface quality in the ultraviolet region.

$\vec{\epsilon}_2$ is decomposed in Fig. 3 according to the transitions starting from VB1, VB2, and VB3. The distinct minima in the VB3 contribution (solid thin lines in Fig. 3) at ~5 eV and in the VB2 contribution (dashed thin lines in Fig. 3) at ~7.5 eV are due to the gap between CB1 and CB2. Only the VB1→CB1 part of the VB1 contribution appears to be well discernible (dashed-dotted thin lines in Fig. 3). The origin of the peaks is presented in detail in Table I. From Fig. 3 and Table I it is evident that the transitions from VB3 dominate both $\epsilon_{2||}$ and $\epsilon_{2\perp}$, but $\epsilon_{2\perp}$ in particular. Transitions from VB2 cause salient features only in $\epsilon_{2||}$ (peaks *B* and *E*). The calculated $\epsilon_{2||}$ and $\epsilon_{2\perp}$ cross below peaks *D* and *d* at 6.5 eV due to transitions VB3→CB2 close to the crossing of the experimental $\epsilon_{2||}$ and $\epsilon_{2\perp}$ at ~5.9 eV (Fig. 2).

A conspicuous anisotropy appears at around 5 eV due to the wide minimum in $\epsilon_{2\perp}$ and at ~8 eV due to the two-peak (*D*,*E*) versus the essentially one-peak (*d*-*e*) structure in $\epsilon_{2||}$ and $\epsilon_{2\perp}$, respectively (Fig. 2). Five anisotropy regions are found. Below 3.5, 3.5–6.5, 6.5–12, 12–14, and above 14 eV,

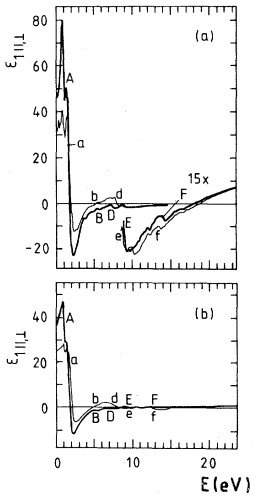

FIG. 4. Real part of the permittivity ($\vec{\epsilon}_1$) of Te. (a) SCOPW $\epsilon_{1||}$ (thick line) and $\epsilon_{1\perp}$ (thin line). (b) Experimental $\epsilon_{1||}$ (thick line) and $\epsilon_{1\perp}$ (thin line) from Ref. 10.

TABLE II. Optical refractive index $n_{||,\perp}=\epsilon_{1||,\perp}^{1/2}$ of Te. Theoretical values obtained at 0 eV and experimental values in the infrared region. Last three columns show the SCOPW $n_{||}$ and $n_\perp$ obtained by taking into account the transitions from one valence-band triplet at a time.

	Experiments			Theory	Contributing triplets VB1	VB2	VB3
$n_{||}$	6.20[a]	6.230[b]	6.02[c]	6.80[d]	1.02	1.53	6.70
$n_\perp$	4.85[a]	4.785[b]	4.76[c]	5.61[d]	1.02	1.49	5.56

[a]Reference 27.
[b]Reference 28.
[c]Reference 29.
[d]Present study.

the anisotropy is mainly due to transitions VB3→CB1, VB2→CB1, VB3 + VB2→CB2, VB1→CB1, and VB2→CB2, respectively (Fig. 3).

We present the calculated $\vec{\epsilon}_1$ (consisting of $\epsilon_{1||}$ and $\epsilon_{1\perp}$, see paper I) and the experimental $\vec{\epsilon}_1$ derived by Bammes *et al.*[10] from the reflectivity measured at 300 K in Figs. 4(a) and 4(b), respectively. We have used for the descending slopes and the concomitant preceding peaks or shoulders in $\vec{\epsilon}_1$ (Fig. 4) the same labels as those for the corresponding peaks in $\vec{\epsilon}_2$ (Fig. 2). Therefore the origin of the main features of $\vec{\epsilon}_1$ can be understood with the aid of the decomposition of $\vec{\epsilon}_2$ (Fig. 3 and Table I). Agreement between the calculated and experimental[10,25,26] $\vec{\epsilon}_1$ is close (see Fig. 4). The calculated and experimental $\epsilon_{1||}$ and $\epsilon_{1\perp}$ cross at almost the same energy of ~8.2 eV. Peaks *A*, *a*, and *d* are higher and the drops (for both polarizations) at about 2.2 and 9.5 eV are deeper in the calculated $\vec{\epsilon}_1$ than in the experimental $\vec{\epsilon}_1$ [agreement below ~5.5 eV is better with the experimental values obtained at the lower temperature of 10 K than with those at 300 K (Ref. 26)].

We compare in Table II the theoretical optical refractive index $n_{||,\perp}=\epsilon_{1||,\perp}^{1/2}$ calculated at 0 eV with the experimental indices[27–29] obtained in the infrared region. The calculated $n_{||}$ and $n_\perp$ are slightly larger than the experimental $n_{||}$ and $n_\perp$, respectively. The facts that the calculated effective number of the valence electrons per atom for $\vec{\epsilon}_2$ ($n_{\text{eff}}=5.8$) is slightly smaller than 6 (see paper I) and that the calculated $n_{||}$ and $n_\perp$ are slightly larger than the experimental $n_{||}$ and $n_\perp$, respectively, independently support the conclusion that the calculated $\vec{\epsilon}_2$ would be slightly concentrated at lower energies. Table II also shows the contribution from VB1, VB2, and VB3 to $n_{||}$ and $n_\perp$. The transitions from VB3 almost alone yield the entire $n_{||}$ and $n_\perp$, reflecting the fact that Te is a small-gap semiconductor. The anisotropy in the optical refractive index is also mainly due to transitions from VB3 (Table II).

The crossing of $\epsilon_{1||}$ and $\epsilon_{1\perp}$ after peaks *D* and *d* (Fig. 4) is mainly due to transitions VB3→CB2. The last zeros of $\epsilon_{1||}$ and $\epsilon_{1\perp}$ appear at 17.8 and 18.6 eV, respectively. This anisotropy in energy is mainly due to transitions VB2→CB2.

We present the calculated reflectivity [consisting of $R_{||}$ and $R_\perp$, Eq. (I.52)] and the reflectivity measured by Bammes *et al.*[10] between 3 and 30 eV at 300 K using the synchrotron radiation in Figs. 5(a) and 5(b), respectively. The same notation is used for the reflectivity peaks in Fig. 5 as that for the corresponding $\vec{\epsilon}_2$ peaks in Fig. 2. Thus the origin of the reflectivity peaks is the same as that of the corresponding $\vec{\epsilon}_2$ peaks (Fig. 3 and Table I). Overall agreement between the calculated and mea-

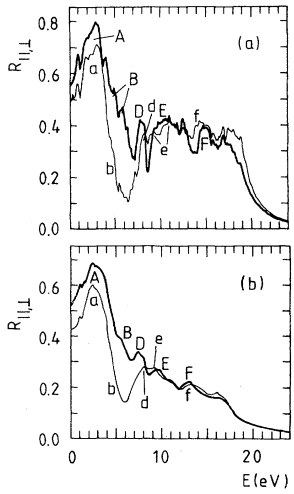

FIG. 5. Reflectivity ($R_{||}$,$R_\perp$) of Te. (a) SCOPW $R_{||}$ (thick line) and $R_\perp$ (thin line). (b) Measured $R_{||}$ (thick line) and $R_\perp$ (thin line) from Ref. 10.

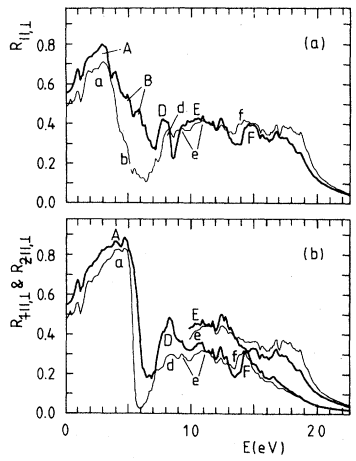

FIG. 6. Valence-band triplet contribution to reflectivity of Te. (a) SCOPW (solid) $R_{||}$ (thick line) and $R_{\perp}$ (thin line). (b) SCOPW reflectivity calculated without VB1 (upper curves), $R_{\not 1||}$ (thick line) and $R_{\not 1\perp}$ (thin line), and without VB2 (lower curves), $R_{\not 2||}$ (thick line) and $R_{\not 2\perp}$ (thin line).

sured[10] reflectivity is good (Fig. 5). Other reflectivity measurements[25,26,30–36] agree fairly well with each other and with the reflectivity by Bammes *et al.*[10] below 12 eV. Peak *B* appears separated out of peak *A* in the calculated $R_{||}$ [Fig. 5(a)], in agreement with $R_{||}$ measured by Tutihasi *et al.*[26] at 10 K. The calculated peak positions are compared with the experimental positions[10,26] in Table I. Agreement is close. The calculated shoulders of $R_{||}$ and $R_{\perp}$ at 17.9 and 18.7 eV, respectively, correspond to the measured shoulders at 16.3 and 16.1 eV, respectively (Fig. 5). These shoulders (plasma edges) are due to the change of sign of $\epsilon_{1||}$ and $\epsilon_{1\perp}$ at 17.8 and 18.6 eV, respectively, which diminishes the reflectivity at higher energies.

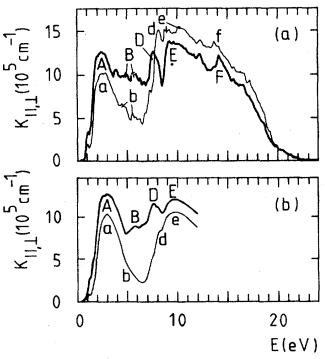

FIG. 7. Absorption coefficient ($K_{||}$,$K_{\perp}$) of Te. (a) SCOPW $K_{||}$ (thick line) and $K_{\perp}$ (thin line). (b) Experimental $K_{||}$ (thick line) and $K_{\perp}$ (thin line) from Ref. 26.

The first peaks of the calculated reflectivity (*A* and *a*, Fig. 5) are slightly higher than those of the measured peaks.[25,26,31,32,34–36] Above ~11 eV the calculated reflectivity is higher than the measured one by a factor of ~2 (Fig. 5). We connect this intensity difference above ~11 eV to that found for $\vec{\epsilon}$ (the calculated $\vec{\epsilon}$ is here smaller than the experimental $\vec{\epsilon}$). It may be possible that surface contamination and/or damage have reduced the intensity of the measured reflectivity in the ultraviolet region (see discussion below).

The reflectivity depends on $\vec{\epsilon}_2$ in an indirect nonlinear way (see paper I). The origin of the anisotropy in the reflectivity can be presented in an illuminating way with the aid of partial reflectivities,[37] which are calculated by omitting the transitions from VB1 or VB2 at a time (denoted by $\not 1$ and $\not 2$, respectively). The resulting curves $R_{\not 1||}$, $R_{\not 1\perp}$, $R_{\not 2||}$, and $R_{\not 2\perp}$ are compared with $R_{||}$ and $R_{\perp}$ in Fig. 6 ($R_{\not 1||}$ and $R_{\not 1\perp}$ are presented only at energies above 10 eV where transitions VB1→CB1 have the main effect). $R_{\perp}$ and $R_{\not 2\perp}$ appear rather similar, indicating that the transitions from VB3 dominate $R_{\perp}$. The shoulders appearing in $R_{||}$ and $R_{\perp}$ at 17.9 and 18.7 eV, respectively, are missing from $R_{\not 2||}$ and $R_{\not 2\perp}$, which shows that the shoulders are fully due to transitions VB2→CB2. The wide minimum in $R_{\perp}$ at around 5 eV and the two- and one-peak structures in $R_{||}$ and $R_{\perp}$, respectively, at ~8 eV form the main anisotropy in the reflectivity (Fig. 5). Below 4, 4–7, 7–12, 12–15, and above 15 eV, the anisotropy is mainly due to transitions VB3→CB1, VB2→CB1, VB3 + VB2→CB2, VB1→CB1, and VB2→CB2, respectively (Fig. 6).

We present the calculated absorption coefficient [consisting of $K_{||}$ and $K_{\perp}$, Eq. (I.53)] and the experimental absorption coefficient derived by Tutihasi *et al.*[26] from the reflectivity measured at 300 K in Figs. 7(a) and 7(b), respectively. The same notation is used for the peaks in Fig. 7 as that for the corresponding $\vec{\epsilon}_2$ peaks in Fig. 2. Thus the origin of the peaks is the same as that of the corresponding $\vec{\epsilon}_2$ peaks (Fig. 3 and Table I). The calculated and experimental[25,26] absorption coefficients agree closely (see Fig. 7). The experimental $K_{||}$ and $K_{\perp}$ do not cross thus apparently violating the sum rule, which requires that the area surrounded by the curve and the energy axis is the same for both polarizations [the areas for the calculated $K_{||}$ and $K_{\perp}$ are the same ($n_{\text{eff}}=5.7$ for both, see paper I)]. The calculated $K_{||}$ and $K_{\perp}$ cross at 7.7 eV. Therefore the calculated $K_{\perp}$ is around 10 eV higher than the experimental $K_{\perp}$ by a factor of ~1.5 (Fig.

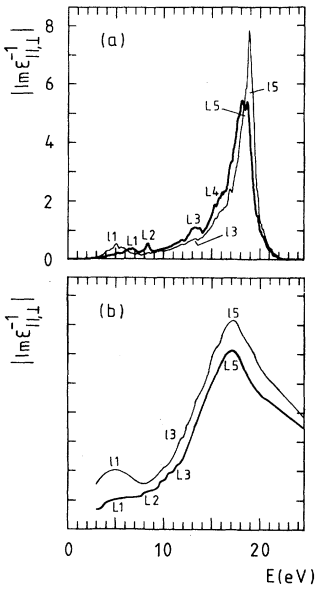

FIG. 8. Electron-energy-loss function ($|\mathrm{Im}\epsilon_{||}^{-1}|$, $|\mathrm{Im}\epsilon_{\perp}^{-1}|$) of Te. (a) SCOPW $|\mathrm{Im}\epsilon_{||}^{-1}|$ (thick line) and $|\mathrm{Im}\epsilon_{\perp}^{-1}|$ (thin line). (b) Measured $|\mathrm{Im}\epsilon_{||}^{-1}|$ (thick line) and $|\mathrm{Im}\epsilon_{\perp}^{-1}|$ (thin line) from Ref. 10 (arbitrary units).

7). The calculated peak positions are compared with the experimental ones[26] in Table I. Agreement is close. The anisotropy regions in the absorption coefficient are the same as those in $\overleftrightarrow{\epsilon}_2$ (see above).

We present the calculated and measured[10] electron-energy-loss functions (consisting of $|\mathrm{Im}\epsilon_{||}^{-1}|$ and $|\mathrm{Im}\epsilon_{\perp}^{-1}|$, see paper I) in Figs. 8(a) and 8(b), respectively. The calculated peak positions [(in eV), 6.8 ($L1$), 8.5 ($L2$), 13.3 ($L3$), ~16 ($L4$), ~18.5 ($L5$), 5.1 ($l1$), 13.3 ($l3$), ~18.8 ($l5$)] agree well with those measured by Bammes *et al.*[10] [(in eV) ~6 ($L1$), 8 ($L2$), 11.5 ($L3$), 17.3 ($L5$), 5 ($l1$), 12 ($l3$), 17.3 ($l5$)]. Shevchik *et al.*[38] obtained the close value of 17.4 eV for the average position of peaks $L5$ and $l5$ from experiments for crystalline films. Both the calculated and measured single plasma peaks ($L5$ and $l5$) appear at higher energies than the free-electron plasma frequency of 15.6 eV, which is consistent with the theory by Pines.[39]

The calculated $|\mathrm{Im}\epsilon_{||}^{-1}|$ and $|\mathrm{Im}\epsilon_{\perp}^{-1}|$ cross twice [at 6.3 and 18.4 eV, Fig. 8(a)] and satisfy accurately the sum rule ($n_{\mathrm{eff}}=5.8$ for both, see paper I), whereas the measured $|\mathrm{Im}\epsilon_{||}^{-1}|$ and $|\mathrm{Im}\epsilon_{\perp}^{-1}|$ do not cross in the measured energy region, thus violating the sum rule [Fig. 8(b)]. On the other hand, $|\mathrm{Im}\epsilon_{||}^{-1}|$ and $|\mathrm{Im}\epsilon_{\perp}^{-1}|$ derived by Bammes *et al.*[10] from the measured reflectivity cross at about 5.8 and 16.8 eV close to the crossings of the calculated $|\mathrm{Im}\epsilon_{||}^{-1}|$ and $|\mathrm{Im}\epsilon_{\perp}^{-1}|$.

The calculated electron-energy-loss function is much higher than that derived from the measured reflectivity.[10] The calculated plasma peaks $L5$ and $l5$ in particular are higher than the derived peaks[10] by a factor of about 3 and 4, respectively. This difference is of the same origin as those found for $\overleftrightarrow{\epsilon}$ and the reflectivity in the ultraviolet region between the calculation and experiment (see discussion below).

The anisotropy below 6.5, 6.5—12, 12—14, and above 14 eV, is due to transitions VB2→CB1, VB3 + VB2→CB2, VB1→CB1, and VB2→CB2, respectively (cf. Fig. 3).

We find a few essential differences between the present SCOPW spectra and the EPSP $\overleftrightarrow{\epsilon}_2$ by Maschke[6] and the SCPSP spectra by Starkloff and Joannopoulos.[7] The EPSP $\overleftrightarrow{\epsilon}_2$ (limited below ~11 eV) is zero at about 5.5—7 eV, and it does not show the two- and one-peaked structure in $\epsilon_{2||}$ and $\epsilon_{2\perp}$, respectively, at ~8 eV, found in both the SCOPW and the experimental[10] $\overleftrightarrow{\epsilon}_2$. In gross features the SCOPW spectra agree fairly well with the SCPSP spectra calculated at 0—13 eV. However, our interpretation for the main anisotropy of the optical spectra at about 5 and 8 eV differs from that of the SCPSP study. In the SCPSP study the anisotropy in the reflectivity at around 5 eV was connected with the anisotropy in $\overleftrightarrow{\epsilon}_2$ at ~8 eV, and it was concluded that both anisotropies originated from transitions VB2→CB2. According to the SCOPW study the anisotropy in all the optical spectra at about 5 and 8 eV is due to transitions VB2→CB1 and VB3 + VB2→CB2, respectively (see Table I and Figs. 3 and 6).

The optical properties of trigonal Se have recently been analyzed in terms of the transitions between the band groups.[12] The notation for the peaks in the spectra of Te and Se is the same, facilitating the comparison. The overall anisotropy is smaller in the spectra of Te than in those of Se [however, the anisotropy in the measured electron-energy-loss function of Te is exceptionally larger than in that of Se (Ref. 10)]. The transitions contribute to the spectra at lower energies in Te than in Se. The largest shift to lower energies is found in the main contribution of transitions VB2→CB2.

Nizzoli found in his model study that the local-field corrections decreased the calculated zero-frequency $\overleftrightarrow{\epsilon}_1$ of Te (Ref. 13) and Se (Ref. 40) by a factor of ~2. Close agreement of the SCOPW spectra of Te and Se (Ref. 12) with the experimental spectra in the entire energy region indirectly

corroborates the conclusion that the local-field effects in Te and Se should be much smaller than those calculated by Nizzoli.[13,40]

The local-field and continuum-exciton corrections increased the calculated zero-frequency $\vec{\epsilon}_1$ of Si (Ref. 15) and TlCl (Ref. 16) and the calculated first (lower-energy) peak in $\vec{\epsilon}_2$ of C,[14] Si,[15] and TlCl,[16] thus improving agreement with experiment. In the SCOPW study of Te the zero-frequency $\vec{\epsilon}_1$ (Table II) and the height of the first peak (*A* or *a*) in $\vec{\epsilon}_2$ (Fig. 2) calculated without the local-field and continuum-exciton corrections are somewhat larger than the corresponding experimental values. Therefore we conclude for Te, parallel to the conclusions drawn for Se,[12] ZrS_2,[17,41] and $ZrSe_2$,[17] that for even closer agreement with experiments at lower energies the corrections needed for the *ab initio* spectra of Te should be opposite to the calculated local-field and continuum-exciton corrections for C,[14] Si,[15] and TlCl.[16]

We found above that in the ultraviolet region the calculated reflectivity and electron-energy-loss function were higher than the measured reflectivity and the associated derived electron-energy-loss function, respectively. Similar differences have been found by Louie *et al.* in the EPSP study for Si,[18] Sturm in the EPSP study for Si, Ge, GaP, GaAs, InAs, and InSb,[19] Wang and Klein in the *ab initio* SC linear combination of Gaussian orbital (LCGO) study for Si, Ge, GaP, GaAs, ZnS, and ZnSe,[20] and Isomäki and von Boehm in the *ab initio* SCOPW study for Se (Refs. 12 and 37) and $ZrSe_2$.[17] An apparent obscurity in the comparison between the calculations and the experiments is caused by the fact that the measured primary plasma peaks (obtained directly from the electron-energy-loss measurements) for Si, Ge,[42] GaP, GaAs, InAs, and InSb (Ref. 43) are higher by a factor of ~ 3 or more than those derived from the measured reflectivities. This disagreement between different experiments may be due to surface contamination and/or damage which are known to reduce the intensity (and possibly also to wipe out salient features) of the measured reflectivities and the associated derived electron-energy-loss functions of Si, Ge, GaP, GaAs, InAs, and InSb.[42–52] Therefore the measured primary electron-energy-loss data should be preferred at high energies. The heights of the plasma peaks calculated by Wang and Klein[20] in the *ab initio* SCLCGO study for Si, Ge, GaP, and GaAs are already without local-field corrections in rather close agreement with the primary measured heights.[42,43] In fact, the calculated large, lowering EPSP local-field corrections for Si,[18,19] Ge, and GaAs (Ref. 19) would considerably worsen this agreement. (Hanke and Sham[15] noted, however, that the calculated continuum-exciton corrections would again enhance the plasma peak of Si). We found that the calculated electron-energy-loss function (without local fields) of Te as well as those of Se (Ref. 12) and $ZrSe_2$ (Ref. 17) agree closely with the measured primary loss functions. This agreement seems to indicate that the local-field effects are small. Hence the difference between the calculated spectra and the measured reflectivity and associated derived spectra in the ultraviolet region seems to be mainly due to the sensitivity of the measured reflectivity to surface quality.

The variant estimates found for the corrections needed to improve the one-electron spectra show that there is still much to be learned before even a qualitative picture of the local-field and continuum-exciton effects may be obtained. The SCOPW results for Te, Se,[12,37] ZrS_2,[17,41] and $ZrSe_2$ (Ref. 17) show that it is possible to calculate one-electron spectra that agree well with the experimental spectra in the entire energy region provided that the band-structure properties and the momentum matrix elements are calculated accurately. Our experience is that the local theories underestimate the smallest transitions,[17] enhancing the optical spectra at lower energies, and that the different convergence rates of distant bands extend and modify the spectra at higher energies.

III. CONCLUSIONS

In this study the permittivity, reflectivity, absorption coefficient, and electron-energy-loss spectra of trigonal Te are calculated in the entire energy region using the self-consistent Hartree-Fock-Slater energy bands and the matrix elements rigorously evaluated in the bulk of the first Brillouin zone. Agreement with experiment is close. All optical spectra for both polarizations are formed of a large peak at ~ 2 eV due to transitions VB3$\rightarrow$CB1. The main anisotropy appears at about 5 and 8 eV due to transitions VB3$\rightarrow$CB1 and VB3 + VB2$\rightarrow$CB2, respectively. The transitions from VB3 dominate all spectra. The transitions from VB2 cause conspicuous peaks (*B*,*E*) only in the parallel optical spectra. Transitions VB1$\rightarrow$CB1 cause peaks (*F* and *f*) at high energies. (The contribution of transitions VB1$\rightarrow$CB2 is negligible.)

By comparing the calculated with the experimental spectra we found that the local-field correc-

tions in the optical refractive index should be much smaller than those calculated recently.[13] We also found that for even closer agreement with experiment at lower energies, the corrections needed for the *ab initio* spectra of Te should be opposite from the calculated local-field and continuum-exciton corrections for C,[14] Si,[15] and TlCl.[16] We found that in the ultraviolet region the calculated reflectivity and electron-energy-loss function were higher than the measured reflectivity and the associated derived electron-energy-loss function, respectively. This difference [and possibly similar ones found for Se,[12,37] $ZrSe_2$,[17] Si,[18–20] Ge, GaP, GaAs,[19,20] InAs, InSb,[19] ZnS, and ZnSe (Ref. 20)] may be to a larger extent related to the sensitivity of the measured reflectivity to the surface quality than to the deficiencies in the one-electron theory.

ACKNOWLEDGMENTS

Two of us (H.I. and J.v.B.) would like to thank Professor M. A. Ranta for his support. We thank Professor T. Tuomi for fruitful discussions. The work of H.I. and J.v.B. was supported by the Academy of Finland.

[1]P. Grosse, in *Springer Tracts in Modern Physics,* edited by G. Höhler (Springer, Berlin, 1969), Vol. 48.
[2]*The Physics of Selenium and Tellurium,* Vol. 13 of the *Springer Series in Solid-State Sciences,* edited by E. Gerlach and P. Grosse (Springer, Berlin, 1979).
[3]H. Ehrenreich and M. H. Cohen, Phys. Rev. 115, 786 (1959).
[4]S. L. Adler, Phys. Rev. 126, 413 (1962).
[5]N. Wiser, Phys. Rev. 129, 62 (1963)
[6]K. Maschke, Phys. Status Solidi B 47, 511 (1971).
[7]Th. Starkloff and J. D. Joannopoulos, Phys. Rev. B 19, 1077 (1979).
[8]H. Isomäki and J. von Boehm, J. Phys. C 13, L485 (1980).
[9]H. Isomäki, J. von Boehm, P. Krusius, and T. Stubb, Phys. Rev. B 22, 2945 (1980).
[10]P. Bammes, R. Klucker, E. E. Koch, and T. Tuomi, Phys. Status Solidi B 49, 561 (1972).
[11]H. M. Isomäki and J. von Boehm, Phys. Scr. 25, 801 (1982).
[12]H. M. Isomäki, Phys. Rev. B 26, 4485 (1982).
[13]F. Nizzoli, J. Phys. C 11, 673 (1978).
[14]W. Hanke and L. J. Sham, Phys. Rev. B 12, 4501 (1975).
[15]W. Hanke and L. J. Sham, Phys. Rev. B 21, 4656 (1980).
[16]W. Schäfer and M. Screiber, Solid State Commun. 38, 1241 (1981).
[17]H. M. Isomäki and J. von Boehm, preceding paper, Phys. Rev. B 26, 5807 (1982) (paper II).
[18]S. G. Louie, J. R. Chelikowsky, and M. L. Cohen, Phys. Rev. Lett. 34, 155 (1975).
[19]K. Sturm, Phys. Rev. Lett. 40, 1599 (1978).
[20]C. S. Wang and B. M. Klein, Phys. Rev. B 24, 3417 (1981).
[21]J. von Boehm and H. M. Isomäki, this issue, Phys. Rev. B 26, 5798 (1982) (paper I).
[22]J. von Boehm and H. Isomäki, in *Recent Developments in Condensed Matter Physics,* edited by J. T. Devreese, L. F. Lemmens, V. E. Van Doren, and J. Van Royen (Plenum, New York, 1981), Vol. 3, p. 287.
[23]Th. Starkloff and J. D. Joannopoulos, J. Chem. Phys. 68, 579 (1978).
[24]M. Schlüter, J. D. Joannopoulos, M. L. Cohen, L. Ley, S. P. Kowalczyk, R. A. Pollak, and D. A. Shirley, Solid State Commun. 15, 1007 (1974).
[25]H. Merdy, Ann. Phys. (Paris) 1, 289 (1966).
[26]S. Tutihasi, G. G. Roberts, R. C. Keezer, and R. E. Drews, Phys. Rev. 177, 1143 (1969).
[27]P. A. Hartig and J. J. Loferski, J. Opt. Soc. Am. 44, 17 (1954).
[28]R. S. Caldwell and H. Y. Fan, Phys. Rev. 114, 664 (1959).
[29]M. Selders, M. S. thesis, University of Cologne, 1966 (unpublished), quoted by P. Grosse, Z. Phys. 193, 318 (1966).
[30]V. V. Sobolev, Dokl. Akad. Nauk SSSR, 151, 1308 (1963) [Sov. Phys.—Dokl. 8, 815 (1964)].
[31]J. Stuke and H. Keller, Phys. Status Solidi 7, 189 (1964).
[32]F. de Chelle and H. Merdy, C. R. Acad. Sci. Paris 265B, 968 (1967).
[33]M. Cardona (unpublished), quoted by J. Stuke, in *The Physics of Selenium and Tellurium,* edited by W. C. Cooper (Pergamon, Oxford, 1969), p. 3.
[34]B. Cervelle and C. Lévy, Bull. Soc. Fr. Minéral. Cristallogr. 99, 220 (1976).
[35]R. R. Forberg, M. S. thesis, Massachusetts Institute of Technology, 1977 (unpublished).
[36]A. J. Hall, B. D. Cervelle, and P. R. Simpson, Mineral. Mag. 43, 909 (1980).
[37]H. M. Isomäki and J. von Boehm, Solid State Commun. 41, 765 (1982).
[38]N. J. Shevchik, M. Cardona, and J. Tejeda, Phys. Rev. B 8, 2833 (1973).
[39]D. Pines, Rev. Mod. Phys. 28, 184 (1956).
[40]F. Nizzoli, in *The Physics of Selenium and Tellurium,* Ref. 2, p. 31.

[41]H. M. Isomäki and J. von Boehm, J. Phys. C 14, L1043 (1981).
[42]K. Zeppenfeld and H. Raether, Z. Phys. 193, 471 (1966).
[43]C. von Festenberg, Z. Phys. 227, 453 (1969).
[44]H. Raether, in *Springer Tracts in Modern Physics,* edited by G. Höhler (Springer, Berlin, 1965), Vol. 38.
[45]L. Marton and J. Toots, Phys. Rev. 160, 602 (1967).
[46]H. Raether, Helv. Phys. Acta 41, 1112 (1968).
[47]J. Daniels, C. von Festenberg, H. Raether, and K. Zeppenfeld, in *Springer Tracts in Modern Physics,* edited by G. Höhler (Springer, Berlin, 1970), Vol. 54.
[48]T. M. Donovan, W. E. Spicer, J. M. Bennett, and E. J. Ashley, Phys. Rev. B 2, 397 (1970).
[49]H. R. Philipp, J. Appl. Phys. 43, 2835 (1972).
[50]A. E. Morgan, Surf. Sci. 43, 150 (1974).
[51]P. J. Zanzucchi and M. T. Duffy, Appl. Opt. 17, 3477 (1978).
[52]J. Stiebling, Z. Phys. B 31, 355 (1978).